LITERATURE REVIEW ON VORTEX-INDUCED VIBRATIONS AROUND CIRCULAR CYLINDERS FOR FUTURE INVESTIGATIONS ON WIND-INDUCED VIBRATIONS AROUND TRANSMISSION LINE CONDUCTORS

Vanessa Gonçalves Guedes, vanessag@cepel.br
Carlos Frederico Trotta Matt, cfmatt@cepel.br
Eletric Power Research Center (CEPEL)
Head Office: Avenida Horácio Macedo 354, Cidade Universitária, Ilha do Fundão, Rio de Janeiro, RJ, Brazil, P.O. Box 68007,
Zip Code: 21944-970

Abstract. *Wind-induced vibrations (or aeolian vibrations) on transmission lines conductors are critical problems for safety and reliability of the transmission line. Different types of mechanical vibrations may occur. The most common type corresponds to wind-excited vibrations in the frequency range of 5 Hz to 100 Hz, caused by vortex-shedding; hence named as vortex induced vibrations or VIV. The aerodynamic lift force arising from the periodic shedding of vortices in the wake of the conductor is responsible for its vibrations in a direction transverse to the wind flow. Based on typical values for wind speed, conductor diameter and standard air properties, a simple calculation reveals that the Reynolds number in aeolian vibrations around transmission line conductors lies in the range of 500 to 20,000. The majority of theoretical works on the subject tries to estimate the maximum conductor vibration amplitude as a function of the wind speed based on the energy balance between the power input by the wind and the power dissipated by the conductor. Few works in the field of aeolian vibrations around transmission line conductors have attempted to provide a deeper insight into this complex fluid-structure interaction problem. Several empirical relations for the power input by the wind are available in the literature; however, they are derived from fittings of experimental data obtained from wind-tunnel tests carried out with rigid cylinders rather than transmission line conductors. Thereby, energy balance calculations accomplished with these empirical functions have led to considerable differences in the expected vibration amplitudes. Indeed, there is a current need for more experimental data and for development of suitable methods for numerical simulation of fluid flow around transmission line conductors, due to their own characteristics. This work presents the first step to achieve the mentioned goal, which is to make a literature review with information and relevant experimental data about VIV phenomenon around circular cylinders. In this review it was noticed that dimensionless parameters found in the literature for VIV around circular cylinders are quite different from the ones typically found for aeolian vibrations around transmission line conductors. The highest mass ratio found in the literature was 250, whereas the mass ratio typically found for wind-induced vibrations on transmission line conductors may reach 2350. Other dimensionless parameters related to the VIV phenomenon are also analyzed.*

Keywords*: Vortex induced vibrations, circular cylinders, Aeolian vibrations, transmission line conductors*

Nomenclature

m = structural mass, kg
c = structural damping, N.s/m
k **=** spring constant, N/m
f = frequency, Hz
T = period, s
D = cylinder diameter, m
L = cylinder length, m
H = Axial load tension, N
EI = flexural rigidity, N.m^2
S = Strouhal number, dimensionless
Re = Reynolds number, dimensionless
C_L = lift coefficient, dimensionless
C_A =added mass coeffcient for small transverse oscillations
S_G = Skop-Griffin parameter
A^* = amplitude ratio, dimensionless
m^* = mass ratio, dimensionless
f^* = frequency ratio, dimensionless
U^* = velocity ratio, dimensionless

Greek Symbols

ζ = damping ratio, dimensionless
ϑ = mass parameter, dimensionless
λ^* = wavelength ratio, dimensionless
λ = wavelength, m
ϕ = phase angle, rad
ρ = fluid density, kg/m^3
μ_C = conductor mass per unit length, kg/m

Subscripts/Superscripts

* relative to dimensionless parameters
N relative to natural
A relative to added
d relative to displaced
S relative to the Strouhal number
e relative to the rigid cylinder

1. INTRODUCTION

Wind-induced vibrations (or aeolian vibrations) on transmission lines conductors are critical problems for safety and reliability of the transmission line. Different types of mechanical vibrations may occur (Meynen *et al.*, 2005; Diana *et al.*, 2000). The most common type corresponds to wind-excited vibrations in the frequency range of 5 Hz to 100 Hz, caused by vortex shedding (Meynen *et al.*, 2005); hence named as vortex induced vibrations or VIV. The aerodynamic lift force arising from the periodic shedding of vortices in the wake of the conductor is responsible for its vibrations in a direction transverse to the wind flow. Based on typical values for wind speed, conductor diameter and standard air properties, a simple calculation reveals that the Reynolds number lies in the range of 500 to 20,000. Aeolian vibrations

around transmission line conductors have their own characteristics, which make them slightly different from VIV studies conducted on oscillating circular cylinders. Typical conductors in Brazilian high-voltage transmission lines are composed of aluminum wires helically wrapped around steel core wires; therefore, geometrically, they are quite different from smooth circular cylinders. The conductor diameters lie in the range of 15 mm to 30 mm. They are strung to extremely high tensile loads (frequently in the range of 20 kN to 30 kN) and their ends are clamped at the suspension towers. The distance between two consecutive towers (the span length) varies from 100 m to 1000 m. Because of these high tensile loads and large span lengths, the conductor's frequency spectrum may be considered, in a first approximation, as almost continuous. Two consecutive natural frequencies of a typical conductor are quite close, separated by approximately 0.1 Hz to 0.2 Hz. Thereby, the conductors are often excited into forced resonant vibrations, that is, the shedding frequency is often close to one natural frequency of the conductor. Another intrinsic characteristic of transmission line conductors is that they have very low internal damping. Damping in such structures arises from inter-strand friction among their constituent wires during bending vibrations. The dynamic stresses and strains induced on the wires may become dangerously high, especially at the suspension clamps, leading to fatigue damage with catastrophic consequences such as the complete rupture of the conductor and interruption on the electric energy supply.

The majority of theoretical works dealing with aeolian vibrations around transmission line conductors tries to estimate the maximum conductor vibration amplitude as a function of the wind speed based on the energy balance between the power input by the wind and the power dissipated by the conductor; the latter one may be measured on a laboratory span during self-damping tests (Diana *et al.*, 2000). Few works have attempted to provide a deeper insight into this complex fluid-structure interaction problem with intrinsic characteristics. Several empirical relations for the power input by the wind are available in the literature (Diana and Falco, 1971; Rawlins, 1983; Brika and Laneville, 1996); however, most of them are derived from fittings of experimental data obtained from wind-tunnel tests carried out with rigid cylinders rather than transmission line conductors in uncontrolled conditions of turbulence level and surface roughness. Meynen *et al.* (2005) computed the specific wind power input after the finite-element solution of the Navier-Stokes equations in the presence of a 2-D circular cylinder oscillating transversely to an incoming uniform and laminar flow. Even though the finite element computations of Meynen et al. (2005) were performed for Reynolds numbers far below the range expected for aeolian vibrations, the numerical predictions obtained for the wind power input fell in the middle of the broad range of experimental data.

Experimental methods proposed to measure the power dissipated by transmission line conductors during self-damping tests on a laboratory span do not fix the minimum sensitivities required for sensors and transducers to keep unavoidable measurement noises as small as possible, which have also led to a noticeable spreading out of the data collected by various laboratories around the world (Diana *et al.*, 2000). Due to the aforementioned shortcomings, calculations accomplished with the energy balance principle have led to considerable differences in the expected vibration amplitudes (Meynen *et al.*, 2005). The discrepancies for the maximum conductor vibration amplitude may reach 55%, depending on the author's fitting curve chosen for the wind power input (Guedes and Costa, 2007). A careful investigation on the literature thus reveals that there is a current need for more experimental data and for development of accurate and robust methods for numerical simulation of aeolian vibrations around transmission line conductors, due to their own characteristics. This work presents the first step to achieve the mentioned goal, which is to make a literature review about the state of the art of VIV phenomenon around circular cylinders, gathering the most relevant information and experimental data. During this literature review, the authors noticed that dimensionless parameters found for VIV around circular cylinders are quite different from those typically found for aeolian vibrations around transmission line conductors. The highest mass ratio found in the literature was 250 (Feng, 1968), whereas the mass ratio typically found for wind-induced vibrations on transmission line conductors may reach 2350. Other dimensionless parameters related to the VIV phenomenon such as reduced velocity and frequency ratio are also analyzed. In future investigations, the study described herein will be useful for the selection and/or development of suitable numerical approaches in order to simulate such wind-induced vibrations. It is noteworthy to say that the bibliographic review made here has no intention to be exhaustive. The purpose of the present manuscript is twofold. The first one is to highlight the main experimental contributions related to VIV phenomenon around circular cylinders. The second one is to identify gaps in the literature that require deeper investigation for dealing with aeolian vibrations.

2. VORTEX-INDUCED VIBRATIONS ON CIRCULAR CYLINDERS

Vortex shedding behind bluff bodies arises in many fields of engineering, such as heat exchanger tubes, marine cables, flexible risers in petroleum production and other marine applications, bridges, chimneys stacks and transmission line conductors. These examples are only a few of a large number of problems where vortex-induced vibrations are important (Williamson and Govardhan, 2004). According to Brankovic and Bearman (2006) vortex induced vibration can severely limit the operation of structures and may even lead to catastrophic failures, such as the well-known collapse of the Tacoma-Narrow bridge in 1940 due to severe wind-induced vibrations.

The case of an elastically mounted (rigid and/or elastic) cylinder vibrating in a cross flow is the most basic and revealing case in the general subject of vortex-induced vibrations around bluff bodies (Sarpkaya, 2004). For the elastically mounted cylinder, two different situations have been widely studied over the past years. One is the free vibration of the cylinder due to the flow-induced forces created by the shed vortices and the other one is the forced vibration of the cylinder. Forced vibrations of the cylinder can be mechanically applied or they may be induced by

upstream vortices (Williamson and Roshko, 1988). In the forced vibration case, if the cylinder is elastic, there will be vortex-induced vibrations superposed on the forced vibration. Contrary, if the cylinder is perfectly rigid, the problem will be dominated by the imposed oscillation frequency. The lock-in or lock-on phenomenon arises when the forcing frequency (equal to the body oscillation frequency) becomes close to the shedding frequency (Bearman, 1984). On the other hand, in the earlier free vibration studies, the lock-in phenomenon, also referred to as resonance or synchronization by some investigators, was defined as the matching between the shedding frequency and the natural frequency of the combined fluid-cylinder system (Griffin and Koopmann, 1977; Sarpkaya, 2004). Indeed, for a high mass ratio, the lock-in or synchronization traditionally means that the frequency ratio $f^* = f / f_N$ remains close to unity. However, as evidenced by Williamson and Govardhan (2004), for light bodies in water, the large amplitude vibrations were verified for a frequency distinctly higher than the natural frequency. The departure of f^* from unit, through lock-in regime, was experimentally shown by Moe and Wu (1990) and Khalak and Williamson (1999). Thereby, lock-in or synchronization is currently defined as the matching of the frequency of the periodic wake vortex mode with the body oscillation frequency (Williamson and Govardhan, 2004). Bearman (1984) analyzed the results derived from both the free and forced vibration tests. Forced vibration tests have the advantage that the reduced velocity and amplitude ratio can be chosen independently; on the other hand, in free vibration tests, these two parameters are coupled, i.e., a change in reduced velocity leads to a change in the amplitude ratio. The disadvantage of the forced vibration tests is that the combinations adopted for the reduced velocity and amplitude ratio are rarely reproduced during free vibration tests.

Table 1 summarizes the dimensionless parameters widely used in the literature for the investigation of vortex-induced vibrations around circular cylinders. These dimensionless parameters will be referenced henceforth until the end of the manuscript. Table 1 also presents the symbol and an expression for the computation of each dimensionless parameter. The reader should refer to the nomenclature section for the description of each symbol appearing in the expressions provided in Table 1.

Table 1. Dimensionless parameters for vortex-induced vibrations around circular cylinders.

Dimensionless parameter	Symbol	Expression
Mass ratio	m^*	$\dfrac{m}{\pi \rho D^2\, L/4}$
Damping ratio	ζ	$\dfrac{c}{2\sqrt{k(m + m_A)}}$
Added mass	m_A	$C_A\, m_d$
Displaced fluid mass	m_d	$\dfrac{\pi \rho D^2 L}{4}$
Reduced or normalized velocity	U^*	$\dfrac{U}{f_N D}$
Wavelength ratio	λ^*	$\dfrac{U}{f_c D}$
Amplitude ratio	A^*	$\dfrac{A}{D}$
Frequency ratio	f^*	$\dfrac{f}{f_N}$
Mass parameter	ϑ	$\dfrac{\rho D^2}{8\pi^2 S^2 m}$
Reduced damping or Skop-Griffin parameter	S_G	$2\pi^3 S^2 (m^* \zeta)$

Wind-induced vibrations around transmission line conductors are expected for wind speeds U in the range of 0.5 m/s to 10 m/s. Considering transmission line conductors, in a first approximation, as circular cylinders, for the Reynolds number range expected for aeolian vibrations (500 – 20,000) one may adopt the Strouhal number S constant and equal to 0.22 (Meynen *et al.*, 2005). Tabs. 2 and 3 show the numerical values computed for the mass ratio m^*, the product $m^*\zeta$ and the Skop-Griffin parameter S_G, for typical values of conductor diameter D, damping ratio ζ and mass per unit length μ_C, where $m = \mu_C \times L$. The mass ratio m^* was computed by assuming a specific mass for the standard air, ρ, equal to 1.24 kg/m³. The conductor damping ratio ζ may be indirectly estimated from logarithmic decrements measured during self-damping tests performed on a laboratory span (Diana *et al.*, 2000). Note that transmission line conductors have indeed a very low internal damping, with a damping ratio varying from 10^{-4} to 10^{-3} in the frequency

range expected for aeolian vibrations (Diana *et al.*, 2000). Transmission line conductors possess many natural frequencies in the frequency range expected for aeolian vibrations. The natural frequencies of a typical conductor may be accurately estimated with the aid of the well-known formula for the natural frequencies of an Euler-Bernoulli beam with flexural rigidity *EI*, subjected to an axial tension *H* and simple-supported at both ends (Dhotarad *et al.*, 1978)

$$f_{\mathrm{N},n} = \frac{n\pi}{L}\sqrt{\frac{H}{\mu_C}}\sqrt{\left[1 + \left(\frac{n\pi}{L}\right)^2 \frac{EI}{H}\right]}, \ n = 1, 2, \ldots, \infty. \tag{1}$$

The conductor's natural frequencies excited during aeolian vibrations lie in the range from 5 Hz to 100 Hz.

From the analysis of Table 2, one may conclude that, for aeolian vibrations around transmission line conductors, the mass ratio m^* lies above 2300. A careful investigation on the literature about VIV around circular cylinders reveals that the highest mass ratio found was 250 in the free vibration experiments of Feng (1968) conducted in air. Therefore, experimental research efforts must be made for much higher mass ratio if one is interested in wind-induced vibrations around transmission line conductors. The numerical values for the product $m^*\zeta$ (also referred to as the mass-damping parameter) lie in the range from 0.24 to 2.35, whereas the values for the Skop-Griffin parameter are within the range from 0.58 to 5.829.

Table 2. Numerical values for the dimensionless parameters m^*, $m^*\zeta$ and S_G, for typical values of conductor diameter D, damping ratio ζ and mass per unit length μ_C.

μ_C [kg/m]	D [mm]	ζ	m^*	$m^*\zeta$	S_G
0.5 2.0	15 30	1.0×10^{-4}	2350	0.24	0.58
0.5 2.0	15 30	1.0×10^{-3}	2350	2.35	5.83

Table 3. Dimensionless parameters U^* and Re for typical values of wind speed U and conductor natural frequency f_N expected for wind-induced vibrations.

D [mm]	f_N [Hz]	U [m/s]	Dimensionless parameters	
			U^*	Re
15 30	5.0	0.5	6.67 3.33	498.9 997.8
15 30	5.0	10	133.33 66.67	9977.9 19955.8
15 30	100	0.5	0.33 0.17	498.9 997.8
15 30	100	10	6.67 3.33	9977.9 19955.8

Experimental measurements conducted in both water and air were collected by Skop and Balasubramanian (1997) and put into a plot of peak-amplitude data versus Skop-Griffin parameter S_G, also known as the Griffin plot (Williamson and Govardhan, 2004). These Griffin plots are illustrated in Figures 1 and 2, where experiments conducted on air are denoted by open symbols whereas experiments conducted on water are denoted by closed symbols. There are also illustrated in Figures 1 and 2 best-fit curves proposed by some previous researchers. Large scatter of the data may be verified from both Figure 1 and Figure 2 for low values of S_G. However, for large values of S_G the proposed fitting curves seem to predict reasonably well the experimental data. It is noteworthy to say that, for wind-induced vibrations around transmission line conductors, the associated Skop-Griffin parameter may be as high as 5.8 (see Table 2) and, for such range of S_G, experimental data are not available in the literature. A careful analysis of Table 3 indicates that the values for the reduced velocity U^*, for selected values of conductor diameter D and natural frequencies f_N, may be at least 0.17 and at most 133.3.

Skop and Luo (2001) collected a series of experimental data and put them into the Griffin plot shown in Figure 1. Those authors also provided the following empirical equation for the maximum vibration dimentionless amplitude in terms of the Skop-Griffin parameter (note that S_G combines both m^* and ζ)

$$A^*_{max} = e^{-0.938\,S_G} \tag{2}$$

Sarpkaya (2004) verified that the empirical equation provided by Skop and Luo (2001) did not reproduce quite well the peak amplitude data at large values of S_G. Sarpkaya (2004) proposed thus a new empirical equation to represent more accurately the experimental data at higher values of S_G, which is given by

$$\left(\frac{A_{max}}{D}\right)\frac{1}{\gamma} = 1.12 e^{-1.05\,S_G} = 1.12 \times 0.35^{S_G} \tag{3}$$

The dimensionless factor γ accounts for both the body geometry and boundary conditions at the fixed ends; for example, γ = 1.0 for a rigid cylinder; γ = 1.291 for a pivoted rod; γ = 1.155 for a taut string and γ = 1.305 for a beam simple-supported at both ends. Sarpkaya (2004) also criticizes the use of the mass ratio m* or the mass-damping m*ζ stating that there is no reasonable explanation to obligate one to combine m^* with ζ. However, according to Williamson and Govardhan (2004), the logic in choosing the combined mass-damping parameter relies on an equation obtained by Khalak and Williamson (1999) for the amplitude ratio as a function of the velocity ratio and frequency ratio, reproduced below for convenience.

$$A^* = \frac{1}{4\pi^3} \frac{C_L \sin\phi}{(m^* + C_A)\zeta} \left(\frac{U^*}{f^*}\right)^2 f^* \tag{4}$$
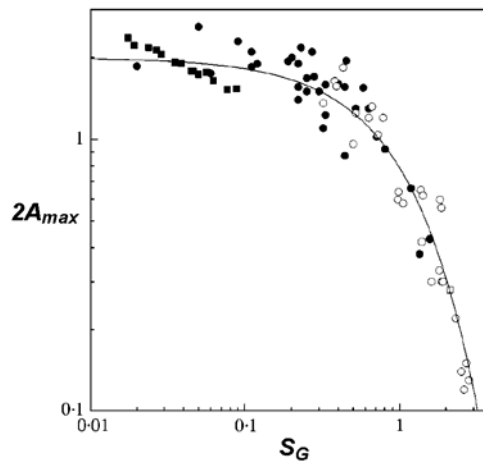
Figure 1 - Peak amplitude data 2Amax versus Skop-Griffin parameter S_G. Open symbols are for experiments conducted in air whereas closed symbols are for experiments conducted in water. ○ and ●: Skop and Balasubramanian (1997); □ Balasubramanian et al. (2000); ■ Khalak and Williamson (1999). The solid curve represents the least-square fit. (from Skop and Luo, 2001).

Bearman (1984) demonstrated that, for large mass ratios, the actual cylinder oscillation frequency, f, at lock-in will be close to the vortex shedding frequency for the static cylinder, f_V, and also close to the system natural frequency f_N, i.e., $f \approx f_V \approx f_N$; hence, $f^* \approx 1$ and the parameter $U^*/f^* = U/f_N D \approx U/fS D = 1/S$, where S is the Strouhal number for the static cylinder, assumed to be constant. Therefore, the assumption is often made that both U^*/f^* and f^* are constants under lock-in conditions, giving the proportional equation (from Eq. (4)):

$$A^* \propto \frac{C_L \sin\phi}{(m^* + C_A)\zeta} \,. \tag{5}$$

As Khalak and Williamson (1999) discussed, if U^*/f^* is assumed constant, then the excitation $C_L \sin\phi$ is a function of the amplitude ratio A^* only. Hence, under these assumptions, one may finally conclude that A* is a function of $(m^* + C_A)\zeta$ only. It should be highlighted that Eq. (5) depends on the earlier assumptions remaining reasonable, namely, $f^* \approx 1$. Based on their own experiments, Khalak and Williamson (1999) finally concluded that, when the mass-damping parameter $m^*\zeta$ is held fixed, the width of the synchronization region is inversely proportional to the mass ratio m^* (i.e., low mass ratio leads to larger synchronization regions, as clearly seen from Figure 3) whereas the maximum vibration amplitude is primarily controlled by the mass-damping parameter, as one can see from Eq. (5). On the other hand, those authors recognized that the discovering of a unique relationship among A^*, m^*, ζ, U^*, f^*, C_L, ϕ and Re remains a problem without solution.
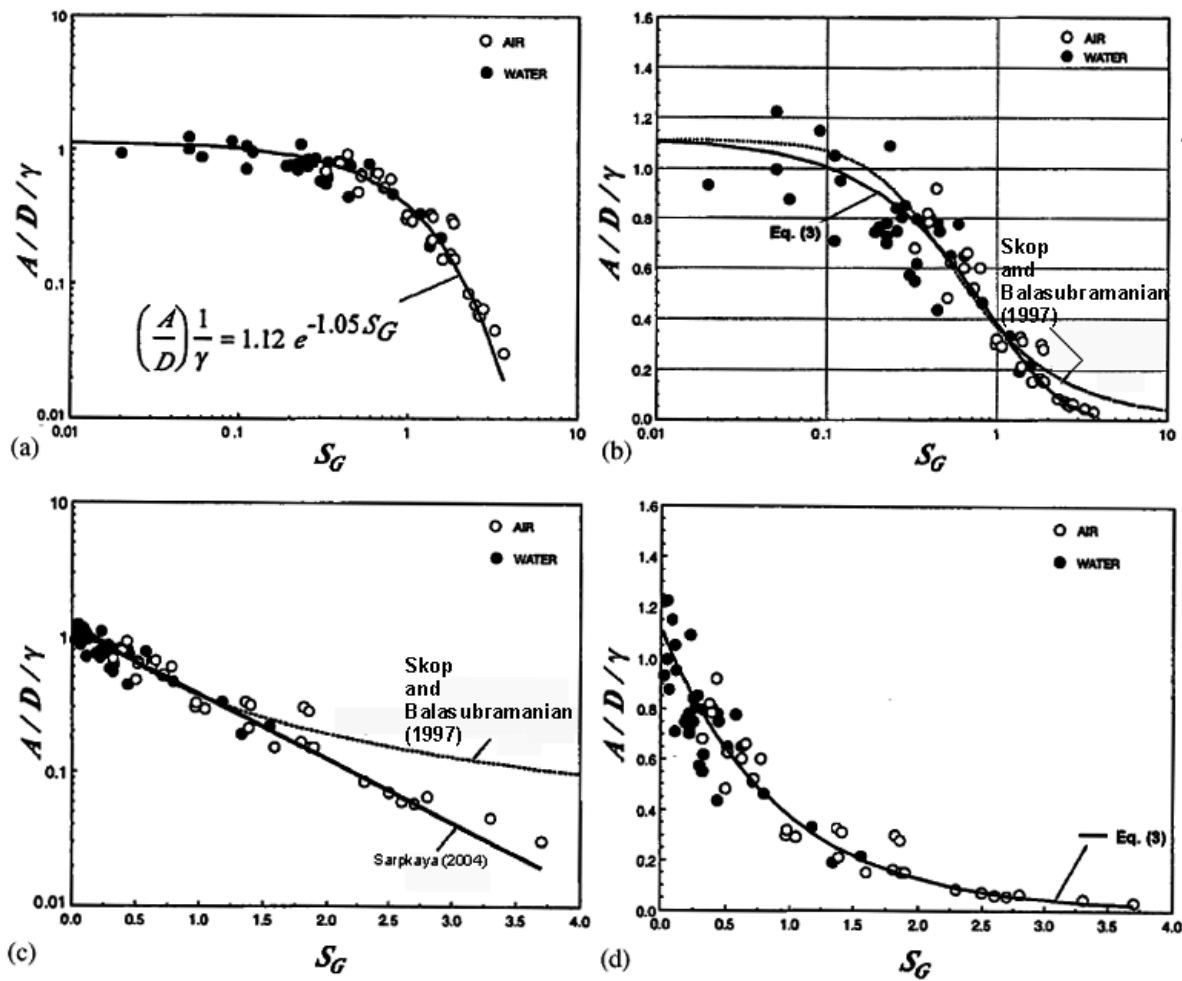
Figure 2 - Peak amplitude data $2A_{max}$ versus Skop-Griffin parameter S_G. Open symbols are for experiments conducted in air whereas closed symbols are for experiments conducted in water (Skop and Balasubramanian ,1997) (a) log–log; (b) linear–log, (c) log–linear and (d) linear–linear (from Sarpkaya, 2004).

Williamson and Roshko (1988) performed a complete and detailed experimental work where they discovered many different wake vortex modes behind a circular cylinder oscillating in a cross flow. Those authors verified experimentally that the well-known synchronization region, where the vortex shedding frequency matches the body oscillation frequency, corresponded to just one kind of wake vortex mode and other synchronization regions were likely to occur. The fundamental synchronization region was discovered to be just one in a series of other synchronization regions, which were completely mapped by Williamson and Roshko (1988) in a wide amplitude-wavelength plane. A description about the synchronization regions discovered by Williamson and Roshko (1988) in the amplitude-wavelength plane will be summarized in the next section. In their experiments, forced oscillations were performed for amplitude ratios up to 6 and for wavelength ratios up to 16, in steps of 0.25 for the former and 1.0 for the latter, although close to the fundamental synchronization region the experiments had been conducted with smaller steps (0.1 for the amplitude ratio and 0.5 for wavelength ratio). The fundamental synchronization region is defined by $0.2 < A/D < 1.8$ and $1.0 < \lambda/D < 10.0$, which corresponds to a body oscillation frequency varying from 0.002 Hz to 0.67 Hz, far below the conductor's natural frequencies commonly excited during wind-induced vibrations. It should be emphasized that the experiments in Williamson and Roshko (1988) were performed for Reynolds numbers between 300 and 1000 in a water tank and, therefore, for mass ratios far below the values computed in Table 2.

At the fundamental lock-in region, Williamson and Roshko (1988) verified that the cylinder acceleration at each half cycle induces the roll-up of two shear layers near the body. These two shear layers interact with each other and the resulting wake comprises a complex mechanism of vortex pairings, which are convected away from the wake centerline. Williamson and Roshko (1988) concluded that changes in this vortex pairing mechanism are the responsible for the transitions between wake oscillation modes. Such changes in the wake oscillation modes coincide with abrupt changes in flow-induced forces acting on the cylinder and with the jump in the phase angle, as previously acknowledged by Bishop and Hassan (1964), Zdravkovich (1982) and Ongoren and Rockwell (1988). Figure 4 shows the abrupt change in the lift force and the jump in the phase angle measured by Bishop and Hassan (1964) during forced

vibration experiments with a circular cylinder oscillating in a water tank. During his free vibration experiments with a high mass ratio, Feng (1968) observed that there is a critical value of the wavelength ratio (or, equivalently, the reduced velocity) for which the jump in phase angle occurs. As shown in Figure 3, the critical wavelength ratio depends on whether the wave length ratio is increasing or decreasing. Feng (1968) also observed an abrupt change in both the flow-induced forces and the amplitude ratio near the critical wavelength ratio.
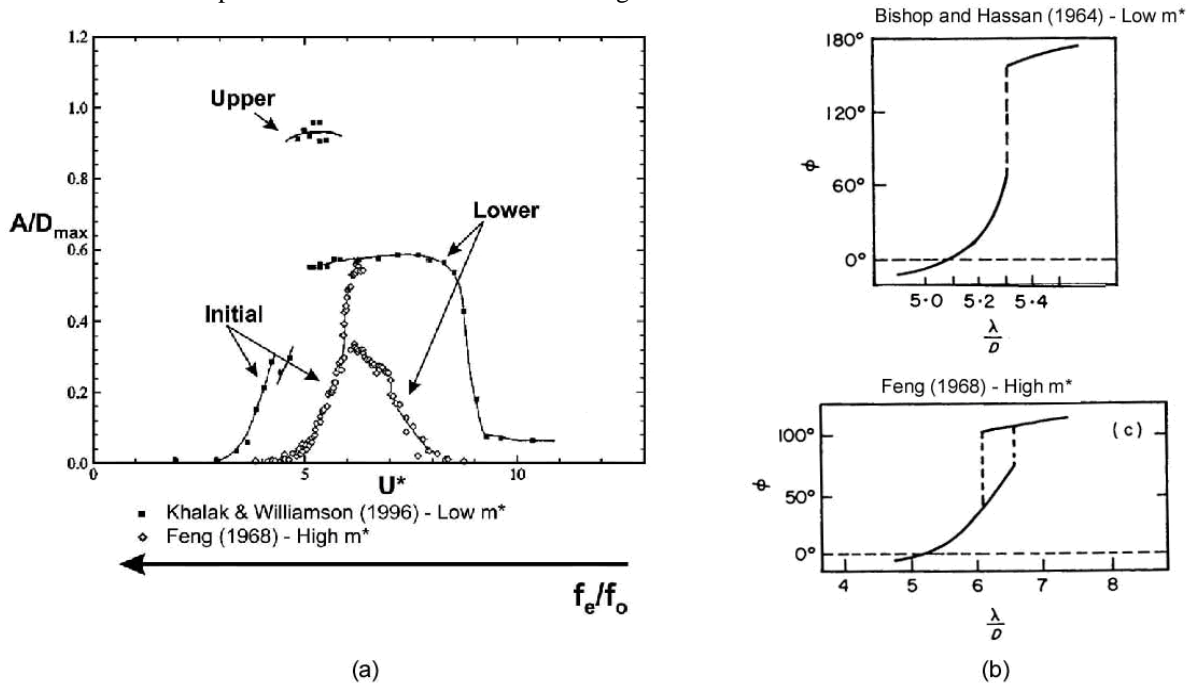
Figure 3 - (a) Amplitude ratio versus reduced velocity U^* for low and high mass ratio m^* during free vibrations; (b) phase angle ϕ versus wavelength ratio for a low mass ratio (forced vibrations, Bishop and Hassan, 1964) and for a high mass ratio (free vibration, Feng, 1968) (adapted from Carberry et al., 2004).
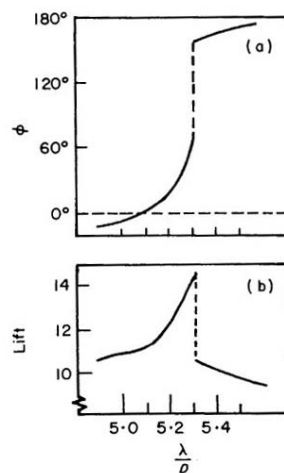
Figure 4 - Phase angle and lift force versus the wavelength ratio measured by Bishop and Hassan (1964) during forced vibration experiments with a circular cylinder oscillating in a water tank.

3. SUMMARY OF THE SYNCHRONIZATION REGIONS IN THE (A/D, λ/D) PLANE

One of the purposes of Williamson and Roshko (1988) was to study the types of wake synchronization that may occur in a much greater region in the (A/D, λ/D) plane that had been studied before (Williamson, 1985; Ongoren and Rockwell, 1988; Stansby, 1976).

In Figs. 5a and 5b, the T_e/T_s horizontal axis, is also shown (approximately) for comparison. The value of T_s is obtained by assuming that the Strouhal number is equal to 0.20 for all investigated Reynolds numbers. The parameter T_e/T_s is related to λ/D by the expression $(T_e/T_s) = S(\lambda/D)$; thus, near the region of fundamental synchronization one has $T_e \cong T_s$ and, consequently, $\lambda/D \cong 5.0$, that is, the cylinder travels about five diameters in each cycle of shedding of vortices.

4. SUMMARY OF THE SYNCHRONIZATION REGIONS IN THE (*A/D*, λ/*D*) PLANE

The sketches presented in Fig. 6 are related to vortex shedding patterns found in the (λ/D, A/D) plane shown in Figs. 5a and 5b. In Fig. 6, P means pair of vortices, S means a single vortex and each pattern is defined by the number of pairs and single vortices shed per cycle; the dotted lines encircles the vortices shed in one complete cycle.

The main vortex shedding patterns near the fundamental lock-in region are 2S, 2P and P+S. The designation 2S means that in each half cycle a single vortex is shed inside the wake downstream, the same way as in the von Karman vortex street; 2P means that in each half cycle a pair of vortices is fed into the wake and is convected laterally away from the centerline, and the P+S mode is an asymmetric version of the 2P mode where a pair of vortices plus a single vortex are shed into the wake every cycle. Other patterns are designed as C(2S) and C(P+S), which means that near the cylinder the pattern is S or P+S but the smaller vortices coalesce with each other immediately behind the body or within 15 diameters, into larger structures. The P and 2P* are related to the patterns named as "single pair" and "two pairs" in Williamson (1985). The P pattern is composed by a pair of vortices shed to the same side, instead of opposite sides, as in the 2P pattern. The 2P* pattern is similar to 2P, but a vortex pair shed in a half cycle is convected downstream, creating a jet. Finally, a 2P+2S pattern looks like the 2P pattern , but with lonely vortices between each vortex pair. This pattern exists near $T_e / T_s \cong 3$ (a 1/3 -subharmonic), without the existence of a pattern at $T_e / T_s \cong 2$ (1/2 -subharmonic).

The empty region in the (λ/D, A/D) plane shown in Fig. 5a between 2P and P+S patterns means that no oscillation pattern characterized by synchronization was identified in Williamson and Roshko (1988) experiments. The limits presented in Fig. 5a may be considered as an approximation. Figure 5b shows the fundamental lock-in region in detail. For $300 < Re < 1000$, the limit between the P+S and the 2P patterns is roughly correct, but for $Re < 300$, the P+S pattern takes place of the 2P mode; the reason for such behavior remains unveiled.

(a)   (b)
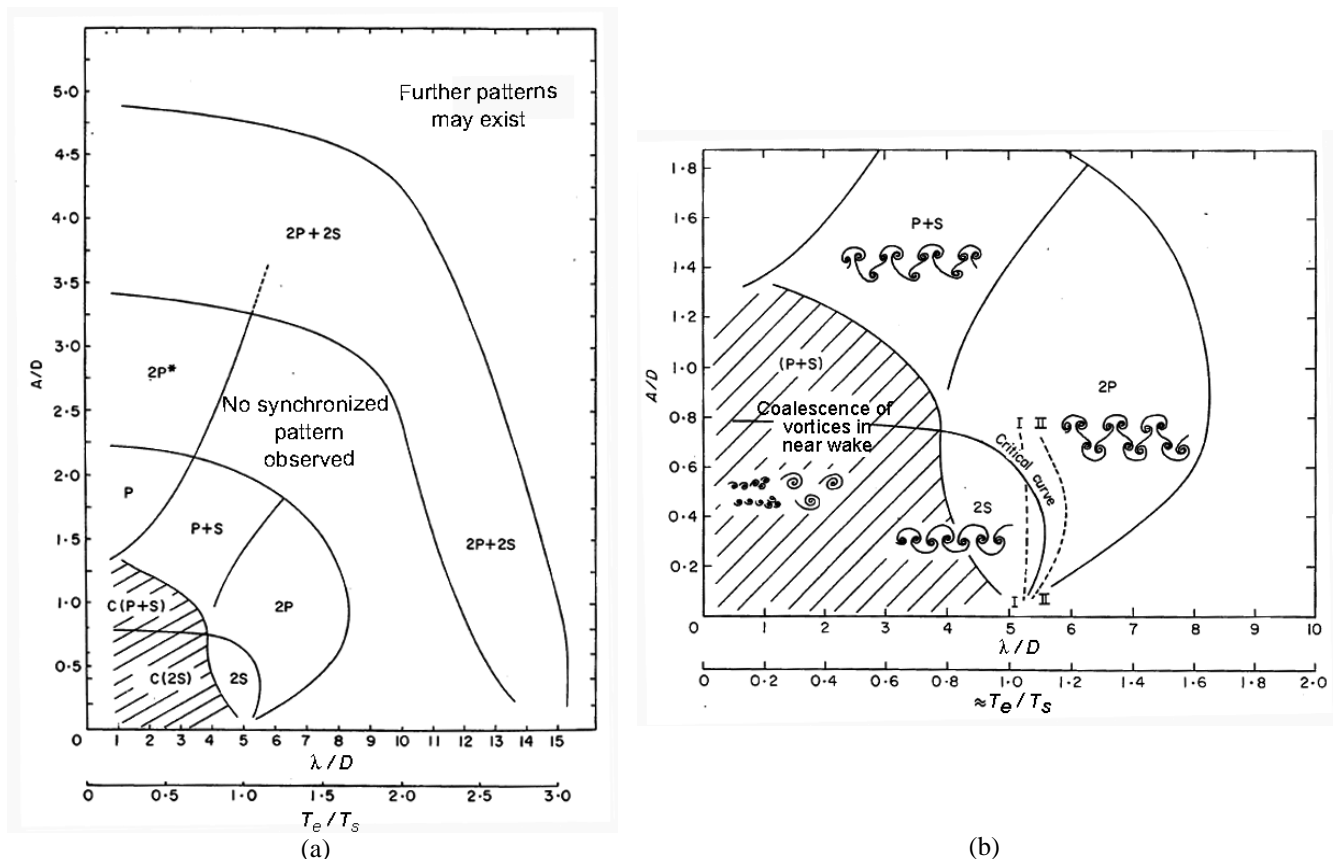
Figure 5– (a) Extended map of synchronization regions in the (λ/D, A/D) plane (extracted from Williamson and Roshko, 1988). (b) Map of synchronization regions in the (λ/D, A/D) plane, near the fundamental lock-in region.

Williamson and Roshko (1988) experiments were performed for Reynolds number between 300 and 1000. The ideal condition would be to keep a fixed Reynolds number to perform the experiments in order to explore the (λ/D, A/D) plane and, afterwards, to repeat these experiments for others Reynolds numbers. Nevertheless, Williamson and Roshko (1988) found more practical to keep the Reynolds number in the range of $300 < Re < 1000$. If one asserts that the vortex dynamics in the near wake is basically inviscid over this range of Reynolds number, one might expect that the vortex formation process is almost similar in the (λ/D, A/D) plane (Williamson and Roshko, 1988).
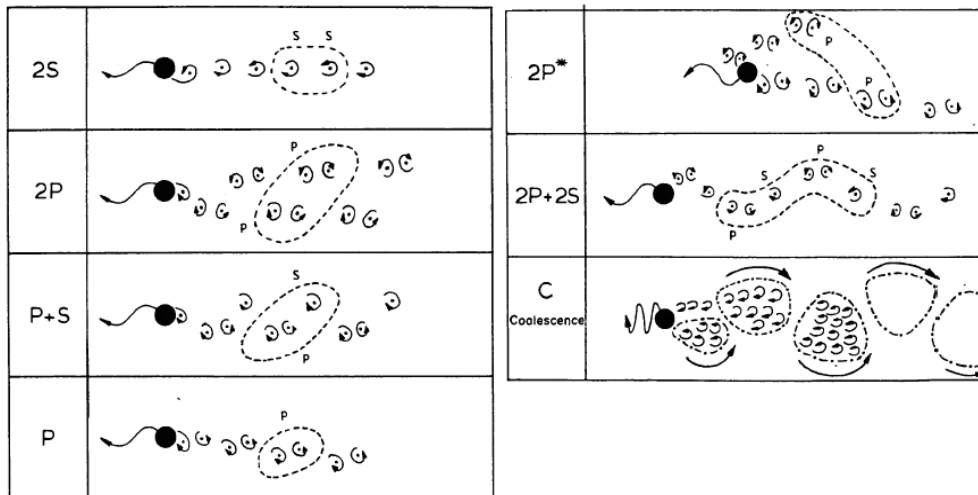
Figure 6 – Vortex shedding patterns mentioned in Figs. 5 and 6; P means pair of vortices; S means a single vortex and each pattern is defined by the number of pairs and single vortices shed by cycle; the dotted lines encircles the vortices shed in one complete cycle (adapted from Williamson and Roshko, 1988).

5. RELATIONSHIP BETWEEN LIFT FORCE AND WAKE PATTERN IN THE FUNDAMENTAL LOCK-IN REGION

The lift force discontinuity is explained by a change in the wake pattern when there is an increase in the wavelength ratio (λ/D). Such changes in the wake pattern also explains the jump in the phase angle shown previously in Figs. 3 and 4. The designed curves I and II shown the Fig. 5b were obtained by Bishop and Hassan (1964), which corresponded to an abrupt change in the lift force behavior. Williamson and Roshko (1988) verified that this change was associated to an abrupt transition from the 2S wake pattern to the 2P wake pattern. The cylinder acceleration in the first half of each cycle causes the roll-up of four regions of vorticity per cycle. Below a critical wavelength ratio, two like-signed vortices amalgamate in each half cycle to create the 2S wake pattern. Above this critical value, vortex amalgamation does not occur and the 2P mode suddenly appears.

6. CONCLUSIONS

The present work provided a bibliographic review concerning the vortex-induced vibrations around freely and forced oscillating circular cylinders. Experimental results were presented in order to show the behavior of the main dimensionless parameters related to the VIV phenomenon for circular cylinders. The present bibliographic review is viewed as a first step to further investigate the aeolian vibrations around transmission line conductors. The majority of theoretical works dealing with aeolian vibrations around transmission line conductors tries to estimate the maximum conductor vibration amplitude as a function of the wind speed based on the energy balance between the power input by the wind and the power dissipated by the conductor. Although several empirical relations for the power input by the wind be available in the literature, most of them are derived from fittings of experimental data obtained from wind-tunnel tests carried out with rigid cylinders rather than transmission line conductors in uncontrolled conditions of turbulence level and surface roughness. Therefore, calculations accomplished with the energy balance principle have led to considerable discrepancies in the expected vibration amplitudes (Meynen *et al.*, 2005). These discrepancies may reach 55%, depending on the author's fitting curve adopted for the wind power input (Guedes and Costa, 2007).

The main goal of the present work was to extend the existing experimental results for VIV around circular cylinders to aeolian vibrations around transmission line conductors by computing the main dimensionless parameters representative of the phenomenon under investigation for typical conductors. The main conclusions are:

⇒ the mass ratio m^* for transmission line conductors lies above 2300; however, the highest mass ratio found in the literature was 250 in the free vibration experiments performed by Feng (1968) in air;

⇒ usually, low mass ratio values were encountered for experiments conducted in water whereas high mass ratios values were encountered for experiments conducted in air;

⇒ as the damping ratio for transmission line conductors lies between 10^{-4} and 10^{-3}, the corresponding Skop-Griffin parameter S_G may be as high as 5.83 (see Tab. 2); however, from the analysis of Figs. 1 and 2, one may conclude that the S_G values for the existing data are at most 5;

⇒ the fundamental lock-in region for circular cylinders corresponds to $0.2 < A/D < 1.8$ and $(1.0 < \lambda/D < 10.0$; such range of λ/D corresponds to a frequency range of 0.002 to 0.67 Hz, far below from the conductors' natural frequencies commonly excited during aeolian vibrations (5 to 100 Hz);

⇒ for a high mass ratio m^*, the system is hysteretic, that is, the exact position of the jump in the phase angle depends whether the wavelength ratio λ/D (or, equivalently, the reduced velocity) is increasing or decreasing.

Taking into account the aforementioned conclusions and the bibliographic review described in the present work, one may ascertain that there is a current need for new studies and experiments on VIV around circular cylinders covering larger ranges for the governing dimensionless parameters in order to apply existing data to aeolian vibrations around transmission line conductors.

7. REFERENCES

Balasubramanian, S., Skop, R. A., Haan, F. L. and Szewczyk, A. A., 2000, "Vortex-excited vibrations of uniform pivoted cylinders in uniform and shear flow", Journal of Fluids and Structures, Vol. 14, pp. 65-85.

Bearman, P. W., 1984, "Vortex shedding from oscillating bluff bodies", Annual Review of Fluid Mechanics, Vol. 16, pp. 195-222.

Bishop, R. E. D. and Hassan, A. Y., 1964, "The lift and drag forces on a circular cylinder in a flowing fluid", Proceedings of Royal Society of London Series A, Vol. 277, pp. 51-75.

Brankovic, M. and Bearman, P. W., 2006, "Measurements of transverse forces on circular cylinders undergoing vortex –induced vibration", Journal of Fluids and Structures, Vol. 22, pp. 829-836.

Brika, D. and Laneville, A., 1996, "A laboratory investigation of the aeolian power imparted to a conductor using a flexible circular cylinder", IEEE Transactions on Power Delivery, Vol. 11, No. 2, pp. 1145-1152.

Carberry, J., Govardhan, R., Sheridan, J., Rockwell, D. and. Williamson C. H. K, 2004, "Wake states and response branches of forced and freely oscillating cylinders", European Journal of Mechanics - B/Fluids, Vol. 23, No. 1, pp. 89-97

Dhotarad, M. S., Ganesan, N. and Rao, B. V. A., 1978, "Transmission Line Vibrations", Journal of Sound and Vibration, Vol. 60, No. 2, pp. 217-237.

Diana, G. and Falco, M., 1971, "On the forces transmitted to a vibrating cylinder by a blowing fluid", Mechanica, Vol. 6, pp. 9–22.

Diana, G., Falco, M., Cigada, A., and Manenti, A., 2000, "On the measurement of overhead transmission lines conductor self-damping", IEEE Transactions on Power Delivery, Vol. 15, pp. 285-292.

Feng, C. C., 1968, "The measurement of vortex-induced effects in flow past a stationary and oscillating circular and D-section cylinders", Master's thesis, University of British Columbia, Vancouver, Canada.

Griffin, O. M. and Koopmann, G.H., 1977, "The vortex-excited lift and reaction forces on resonantly vibrating cylinders", Journal of Sound and Vibration, Vol. 54, pp. 435-448.

Guedes, V. G. and Costa, F. M. F., 2007, Maximum vibration amplitude versus excitation frequency for transmission line conductors, Technical Report No. 2168/07 (in Portuguese), Research Project DIE-1773, Electric Power Research Center, Brazil, 24p.

Khalak, A. and Williamson, C. H. K., 1999, "Motions, forces and mode transitions in vortex-induces vibrations at low mass-damping", Journal of Fluids and Structures, Vol. 13, pp. 813-851.

Meynen, S., Verma, H., Hagedorn, P. and Schäfer, M., 2005, "On the numerical simulation of vortex-induced vibrations of oscillating conductors", Journal of Fluids and Structures, Vol. 21, pp. 41-48.

Moe, G. and Wu, Z.J., 1990, "The lift force on a cylinder vibrating in a current", ASME Journal of Offshore Mechanical Artic Engineering, Vol. 112, pp. 297-303.

Ongoren, A. and Rockwell, D., 1988, "Flow structure from an oscillating cylinder. Part 1: Mechanisms of phase shift and recovery in the near wake", Journal of Fluid Mechanics, Vol. 191, pp. 197-223.

Rawlins, C., 1983, "Model of power imparted to a vibrating conductor by turbulent wind", Technical Report No. 31, Alcoa Conductor Products Company.

Sarpkaya, T., 2004, "A critical review of the intrinsic nature of vortex-induced vibrations", Journal of Fluids and Structures, Vol. 19, pp. 389-447.

Skop, R. A. and Balasubramanian, S., 1997, "A new twist on an old model for vortex-excited vibrations", Journal of Fluids and Structures, Vol. 11, pp. 395-412.

Skop, R. A. and Luo, G., 2001, "An inverse-direct method for predicting the vortex-induced vibrations of cylinders in uniform and non-uniform flows", Journal of Fluids and Structures, Vol. 15, pp. 867-884

Stansby, P. K., 1976, "The locking-on of vortex shedding due to the cross-stream vibration of circular cylinders in uniform and shear flows", Journal of Fluid Mechanics, Vol. 74, pp. 641-665.

Williamson, C. H. K., 1985, "Sinusoidal flow relative to circular cylinders", Journal of Fluid Mechanics, Vol. 155, pp. 141-174.

Williamson, C. H. K. and Roshko, A., 1988, "Vortex formation in the wake of an oscillating cylinder", Journal of Fluids and Structures, Vol. 2, pp. 355-381.

Williamson, C. H. K. and Govardhan, R. ,2004, "Vortex-Induced Vibrations", Annual Review of Fluid Mechanics, Vol. 36, pp. 413-455.

Zdravkovich, M. M., 1982, "Modification of vortex shedding in the synchronization range", ASME Journal of Fluids Engineering, Vol. 104, pp. 513 –517.

8. RESPONSIBILITY NOTICE The authors are the responsible for the printed material included in this paper.